Energy Equip. Sys./ Vol. 6/No. 1/March 2018/ 39-49

ENERGY EQUIPSYS

Energy Equipment and Systems

http://energyequipsys.ut.ac.ir
www.energyequipsys.com

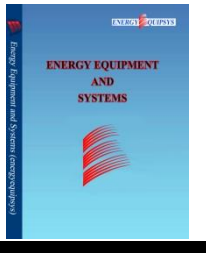

Numerical simulation of turbulent flow around the dtmb4119 propeller in open water conditions

Authors

Amirhossein Niroumand[a]
Amin Ashtari Larki[a]
Mahmoud Abbaszadeh[b*]

[a] Department of Mechanical Engineering, Ragheb Isfahani Higher Education Institute, Isfahan, Iran

[b] School of Engineering, University of Warwick, Coventry, United Kingdom

ABSTRACT

In this study, ANSYS-FLUENT packages are employed to simulate the turbulent flow around DTMB4119 propeller in open water conditions. In order to form a mesh, the multiple reference frame (MRF) methodology is used. The results are compared with the experimental results and a good conformity is obtained, which endorses numerical simulation. Furthermore, the $k-\omega$ *turbulence model is used, which is superior to other turbulence models in modeling marine propellers. The investigation focuses on aspects related to the influence of the pressure coefficient and the advance coefficient on hydrodynamic performance and cavitation of the propeller. The results reveal that the pressure coefficient at first decreases and then augments as it moves from the leading edge to trailing edge in the suction surface. Moreover, by increasing the blade radius and its speed, the minimum pressure increases in a way that pressure coefficient reaches its minimum value. Furthermore, volume fraction of the vapor over the blades decreases as the advance coefficient increases. As a result, the possibility of cavitation decreases.*

Article history:

Received : 26 August 2017
Accepted : 9 December 2017

Keywords: DTMB4119 Propeller, Turbulent Flow, CFD Simulation, Hydrodynamic Performance, Cavitation

1. Introduction

With time, it is incontrovertibly axiomatic that design optimization of the propeller in submarines is a crucial milestone for military designers. It is very important to recognize the fluid flow characteristics around these devices in order to be able to create a better design. One of the most important marine propellers is the DTMB4119 propeller. An issue of concern in these propellers is the distribution of pressure on them and the cavitation in the cavitation in deep oceans. Therefore, a deep understanding of the elaborate DTMB4119 propeller is very important for designers. In recent years, quite a few CFD studies were conducted to recognize the behavior of the flow around the propellers [1–4]. As early as 1978, Kerwin and Lee [5] employed the unsteady vortex lattice technique in order to formulate the unsteady propeller. In another numerical simulation, flow pattern and performance parameters of a DTNSRDC P4119 marine propeller in uniform flow were calculated by Chang [6]. He used the finite volume CFD method and utilized the standard k-ε turbulence model. Unsteady flow around a

* Corresponding author: Mahmoud Abbaszadeh
School of Engineering, University of Warwick, Coventry, United Kingdom
Email: m.abbaszadeh@warwick.ac.uk

high-skewed propeller in non-uniform inflow was examined by Funeno et al. [7]. Hu et al. [8] numerically scrutinized the unsteady thrust and torque of propeller DTMB 4119 in viscous flow. Their considered propeller worked in uniform inflow conditions. In another study [9], two different propellers (DTMB 4119 and SEIUN-MARU highly skewed propeller) were compared by lifting surface and by CFD methods. They concluded that CFD methods can be utilized as a powerful means for pre-design. Huang et al. [10] employed the FLUENT software to simulate the thrust and torque coefficient as a function of the advance coefficient of propeller and thrust efficiency of additional thrust fins. They also calculated the pressure and velocity flow behind the propeller.

As evident in the aforementioned literature, little study has been done to monitor the behavior of the pressure coefficient and cavitation of DTMB 4119 marine propellers. Therefore, in the present study, the FLUENT software was used to simulate the turbulent flow around the DTMB 4119 propeller. Moreover, the Multiple Reference Frame (MRF) methodology is used to create a moving mesh in the problem field. The effects of the advance coefficient in different dimensionless radius were also examined.

Nomenclature

Cp	Pressure coefficient
D	Diameter
G	Gravity acceleration
J	Advance velocity ratio
Kt	Trust coefficient
Kq	Torque coefficient
N	angular velocity (RPM)
P	Pressure
R	Radius
T	Time
V	Velocity
η	Efficiency

2. Problem definition

The problem configuration is depicted in Figure 1. Moreover, a viscid incompressible flow around a DTMB 4119 propeller and its working characteristics were examined. The working characteristics included the trust coefficient, torque, and efficiency of the system in open water conditions. The propeller had three blades with the diameter of 0.3048mm. The geometric characteristics of the propeller are presented in 0Table 1. It is noteworthy that it was possible to conduct the simulation in one-third of geometry when the inlet conditions of the flow were applied uniformly. However, a thorough geometry of the propeller was employed for simulation when the modeling of the flow field was accurate.

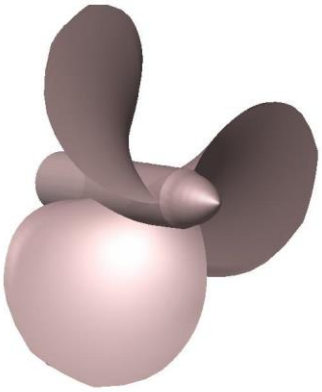

Fig. 1. Schematic of the DTMB-4119 propeller

Table 1. The geometric characteristics of the propeller

Diameter	3048/0
Number of blades	3
Rake	0
Skew angle	0
Blade section	NACA 66 a = 0.8

Table 2. The geometric characteristics of the propeller blades

r/R	Chord	P/D	Thickness
0.2	0.32	1.105	0.2055
0.3	0.3625	1.102	0.1553
0.4	0.4048	1.098	0.118
0.5	0.4392	1.093	0.0916
0.6	0.461	1.088	0.0696
0.7	0.4622	1.084	0.05418
0.8	0.4347	1.081	0.04206
0.9	0.3613	1.079	0.03321
0.95	0.2775	1.077	0.03228
0.98	0.03	1.075	0.0316

2.1. The Hydrodynamic Performance of the Propeller

The propeller systems can be examined under two conditions of open water and its performance on its hinder. The simplest way of examining the propeller in marine science is under open water condition. In this way, the performance of the propeller should be examined in terms of thrust force, the applied torque on the blades, and the efficiency of the propeller in the uniform water condition. The

dimensionless form of the trust force and the torque on the propeller are as follows:

$$K_T = \frac{T}{\rho N^2 D^4} \quad (1)$$

$$K_Q = \frac{Q}{\rho N^2 D^5} \quad (2)$$

where, N is the angular velocity, D is the diameter of the propeller, T is the trust force, and Q is the torque. The hydrodynamic coefficients are usually interpreted on the basis of the leading coefficient of *J,* which is:

$$J = \frac{V}{ND} \quad (3)$$

where, V is the inlet velocity. In open water condition, the efficiency of the propeller (η) was obtained by dividing the produced power (P_T) by the consumed power (P_Q).

$$\eta = \frac{P_T}{P_Q} = \frac{TV}{2\pi NQ} = \frac{JK_T}{2\pi K_Q} \quad (4)$$

2.2. Boundary Conditions

Under open water condition, the inlet velocity was definite and, therefore, the inlet velocity boundary condition is applied uniformly. In the outlet, the constant pressure condition was used as the pressure was known in this boundary. Moreover, the rotation with angular velocity of ω was the boundary condition used for blades and hub. Finally, the outer boundary of the flow was a wall, where the shear stress on it was zero.

2.3. Solution Domain

The solution domain was a cylinder with 5D length and 4D diameters, which is depicted in Fig.2. Moreover, a cylinder was considered around the propeller with 1.1D diameter and 0.4D length as a rotary volume. This was arranged in a way that the propeller was located at the center of this cylinder. The solution filed with its boundaries is illustrated in Fig.3.

In above figures, the solution domain is composed of two zones: the inner zone and the outer zone. The inner zone rotates while the outer zone does not. For the inlet and outlet boundaries, the velocity boundary condition and the pressure boundary were taken into account, respectively. The performance characteristics of the propeller, including the trust force and torque of the propeller, were obtained by solving the flow field with the aim of the FLUENT.

2.4. Mesh Generation

The GAMBIT software [11] was employed to generate mesh, which was a key element in modeling the propeller in the solution domain. The mesh generation consisted of two parts. Although the solution domain was fixed and constant in the first part, the rotatory volume was meshed properly in the second part. Furthermore, the mesh generation should be smaller in spots where the velocity gradient was high enough, such as near the blades and especially in the wake section. This was necessary in order to gain a solution with high accuracy.

Mesh generation began by producing the triangular cells on the blades and the surface of the hub. In this section, the regions near the summit, root, and the edge of the blades were covered by smaller triangles. However, bigger triangles with grow rate of 1.1 were used to cover other surfaces of the propellers. Figure 4 shows the mesh generation of the solution

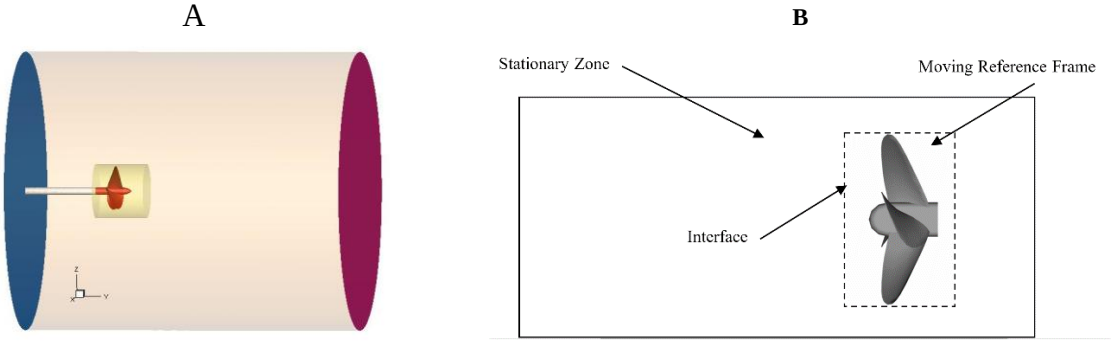

Fig. 2. a)The solution domain with its boundaries; b)Boundary Conditions

domain. In the next section, the tetragonal cells were produced in the solution domain. The solution domain is divided into two or more cylinders in order to gain an optimum mesh.

Mesh generation of some parts of the solution domain are presented in Fig.5 and 0 Fig.6. As can be seen in these figures, the magnitude of the cells became larger when we get away from the blades.

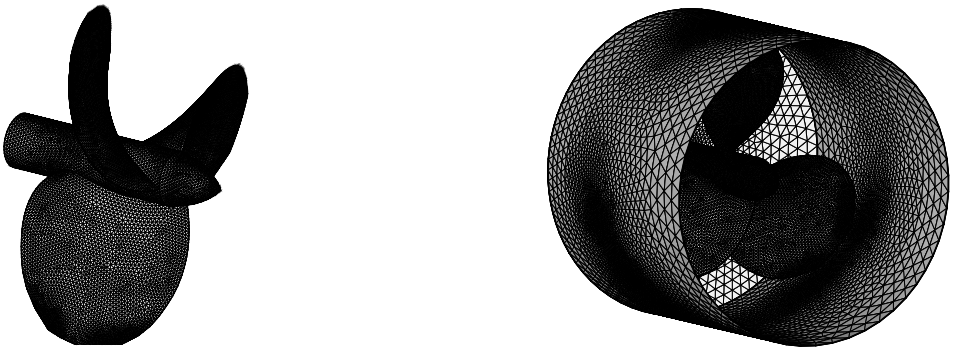

Fig. 4. Mesh generation on the rotatory and fixed zones: a) propeller b) moving zone

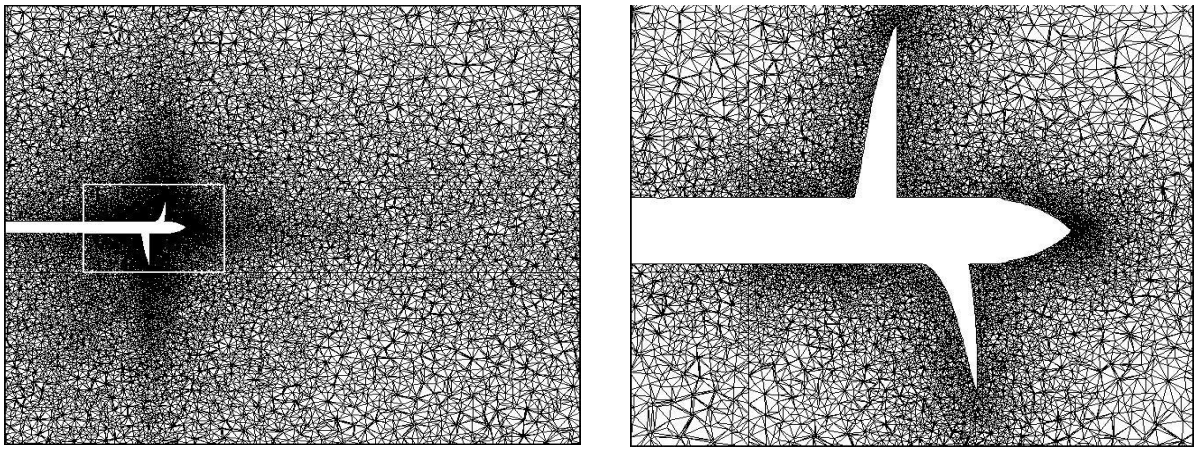

(a) (b)

Fig. 5. (a) mesh generation of a part of the solution domain that is cut by the Z = 0 plane, (b)the magnification of the spot between two blades, which are shown in (a) section

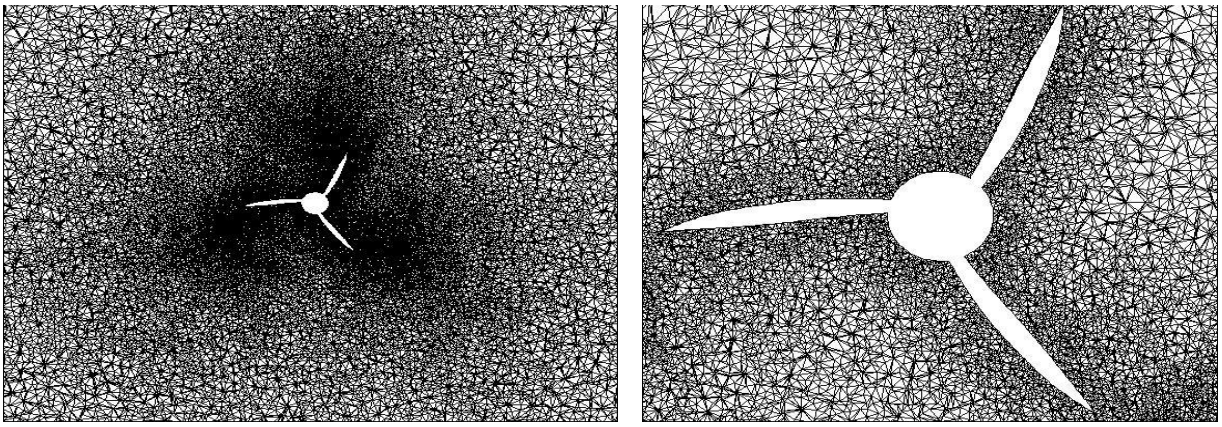

(a) (b)

Fig. 6. (a) mesh generation of a part of the solution domain that is cut by the Y = 0 plane; (b) the magnification of the spot between two blades which are shown in (a) section

3. Numerical Implementation

Numerous turbulence models were developed by different researchers and scholars. Each of them could be used in a certain flow regime and were valid and accurate in certain parts of the domain. Moreover, the two-equation models were cornerstones of quite a few researches regarding turbulent flows in recent years and they were the simplest turbulent models. Two of the well-known two-equation models were $k-\varepsilon$ and $k-\omega$. Most of the simulations achieved using CFD were benefited from the $k-\omega$ method, which was based on the shear stress transfer. However, $k-\varepsilon$ and $k-\omega$ will be explained [12–15].

3.1. *k-ε* Model

The $k-\varepsilon$ model was a well-known two-equation model [16]. In this model, the turbulence field was defined by two parameters: kinetic energy of the turbulent flow and viscous dissipation rate of turbulent kinetic energy. In this model, the turbulent kinetic energy equation is as follows:

$$\rho\frac{Dk}{Dt}=\frac{\partial}{\partial x_i}\left[\left(\mu+\frac{\mu_t}{\sigma_k}\right)\frac{\partial k}{\partial x_i}\right]+ G_k+G_b-\rho\varepsilon-Y_M \tag{5}$$

The equation of the dissipation rate of the energy is:

$$\rho\frac{D\varepsilon}{Dt}=\frac{\partial}{\partial x_i}\left[\left(\mu+\frac{\mu_t}{\sigma_\varepsilon}\right)\frac{\partial \varepsilon}{\partial x_i}\right]+ C_{1\varepsilon}\frac{\varepsilon}{k}(G_k+C_{3\varepsilon}G_b)-C_{2\varepsilon}\rho\frac{\varepsilon^2}{k} \tag{6}$$

where, G_k and G_b is the turbulent kinetic energy produced by the average velocity gradient and buoyancy force, respectively.

$$G_k=\rho\overline{u_i'u_j'}\frac{\partial u_j}{\partial x_i}, \tag{7}$$

$$G_b=\beta g_i\frac{\mu_t}{Pr_t}\frac{\partial T}{\partial x_i} \tag{8}$$

where, G_b is zero as the temperature is constant. Thus, $C_{3\varepsilon}$ did not have any effect on the turbulent model. Y_M is the compensation of dilatory fluctuations of the compressible turbulence from all the dissipative rate of energy. In this study, the flow was incompressible and the value was zero. Here, μt is the turbulence viscosity.

$$\mu_t=\rho C_\mu\frac{k^2}{\varepsilon} \tag{9}$$

$C_{1\varepsilon}$, $C_{2\varepsilon}$, and C_μ are constant. σ_ε and σ_k are the turbulent Prandtl numbers for k and ε, and these values are considered constant in the fluent.

$$C_{1\varepsilon}=1.44, C_{2\varepsilon}=1.92, C_\mu=0.09, \sigma_k=1.0, \sigma_\varepsilon=1.3 \tag{10}$$

3.2. RNG *k-ε* Model

The turbulent RNG $k-\varepsilon$ model was derived from the Navier–Stokes equation, with the aim of renormalization of the group mathematical method [17]. This method was based on the standard $k-\varepsilon$ model and had some advantages. This model had an excessive term in the ε equation, which increased the accuracy of the flow with high velocity. The effects of the rotating vortices in turbulence were presented in this model, which improved the vorticity flow simulation. This model provided one analytical formula for the turbulent Prandtl number, while the $k-\varepsilon$ model used a constant number instead. The *RNG* theory had one analytical formula for the effects of viscosity in low Reynolds numbers, whereas the $k-\varepsilon$ model was for high Reynolds numbers.

In this method, the turbulent kinetic energy equation (k-equation) is as follows:

$$\frac{\partial k}{\partial x_j}=\frac{1}{\rho}\frac{\partial}{\partial x_j}\left[\left(\mu+\frac{\mu_t}{\sigma_k}\right)\frac{\partial k}{\partial x_j}\right]+P_k-\varepsilon \tag{11}$$

Energy dissipation rate equation is as follows:

$$\frac{\partial \varepsilon}{\partial x_i}=\frac{1}{\rho}\frac{\partial}{\partial x_j}\left[\left(\mu+\frac{\mu_t}{\sigma_\varepsilon}\right)\frac{\partial \varepsilon}{\partial x_j}\right]+ C_{1\varepsilon}\frac{\varepsilon}{k}P_k-C_{2\varepsilon}\frac{\varepsilon^2}{k} \tag{12}$$

P_k is the produced turbulent energy, which is defined as follows:

$$P_k=v_t\left(\frac{\partial u_i}{\partial x_j}+\frac{\partial u_j}{\partial x_i}\right)\frac{\partial u_i}{\partial x_j} \tag{13}$$

$C_{1\varepsilon}$, $C_{2\varepsilon}$, and C_μ have aforementioned values.

3.3. The *k-ε* Model

Generally, the turbulent models which were based on the equation suffer from predicting the start of separation rapidly. To surmount this problem, the $k-\omega$ model [18], which was based on the shear stress transfer, was designed to predict with high accuracy under unfavorable gradients. Another advantage of this model was that of improving the equations in low Reynolds numbers near the walls to build up accuracy of the calculations.

In the present study, the used under relaxation coefficient for pressure was 0.3, for momentum it was 0.7, and both of the k and ε was 0.8. Furthermore, the dynamic viscosity and density of water are considered to be 0.001003kg/ (m.s) and 1000kg/ m^3. Moreover, the convergence criterion in this study was considered 10^{-4}.

4. Results and Discussion

4.1. Grid Independency Test

In order to ensure the independency of the numerical results from the grid, three types of grid—fine, medium, and coarse grid—were produced. Table 3 shows comparison between the number of mesh and the foregoing hydrodynamic coefficients. Here, the advance coefficient is 0.4 (the inlet velocity is 1.6m/ s) and the propeller has a rotational velocity of 789rpm. As can be concluded from this table, the finer the grid the lower is the amount of error. Finally, the medium grid was found to be the best grid for the simulation as it had a little difference with other grids and it was also cost-effective in terms of time.

On the other hand, another criterion in examining the accuracy of the grid was the y^+ parameter. This parameter in the rotational flows must be in the interval of $30 < y^+ < 500$. In other words, the appropriate value of y^+ confirmed the high accuracy of the grid near the surface, the boundary layer mesh, and the growth of the mesh near the blades. The y^+ values for J = 1 is displayed in Fig.7.

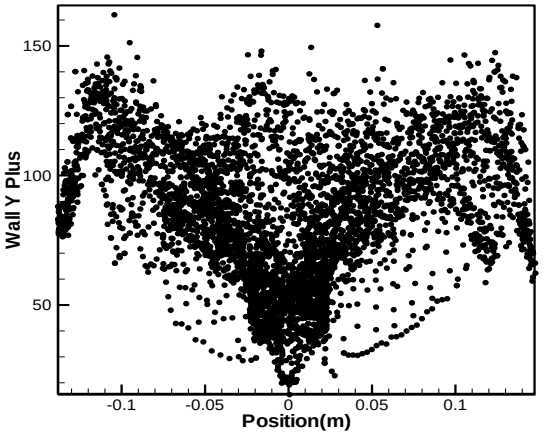

Fig. 7. The y^+ values for J = 1

4.2. Validation of the Results

The hydrodynamic coefficients in terms of advance coefficient for the present study and experimental results are compared in0 Table 3. There was a good conformity between the numerical results and the literature. As can be seen in Table 3, the trust and torque coefficients were close to each other for any values of advance coefficient. Their discrepancy was lower than 9%. However, for the efficiency of the propeller the numerical with experimental results have a deviation that is more clear at the advance coefficients greater than 0.7. Another noteworthy point regarding this figure is that of the efficiency for J = 0.9, which had the maximum value for both the numerical and experimental results. This fact demonstrated that the propeller had the best performance at J = 0.9. Moreover, it is important that for the vibration analysis of the propeller and the effects of solid and fluid, J was considered 0.2. This value generated a good conformity between the numerical and experimental results.

Table 3. Comparisons of the obtained hydrodynamic coefficients for different grids.

Type of grid	Number of mesh (million)	$K_{T,Total}$	$10K_{Q,Total}$	η_{Total}
Coarse	1.520	0.299	0.476	0.399
Medium	2.748	0.301	0.488	0.396
Fine	3.11	0.305	0.493	0.394

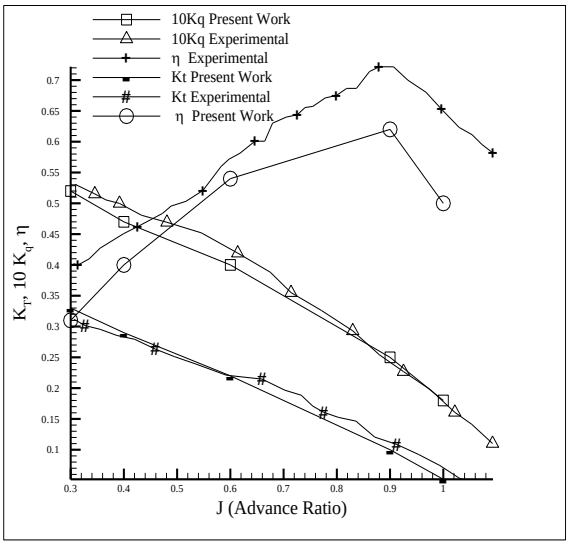

Fig. 8. Comparisons of the present study and the experimental study of Jessup [15].

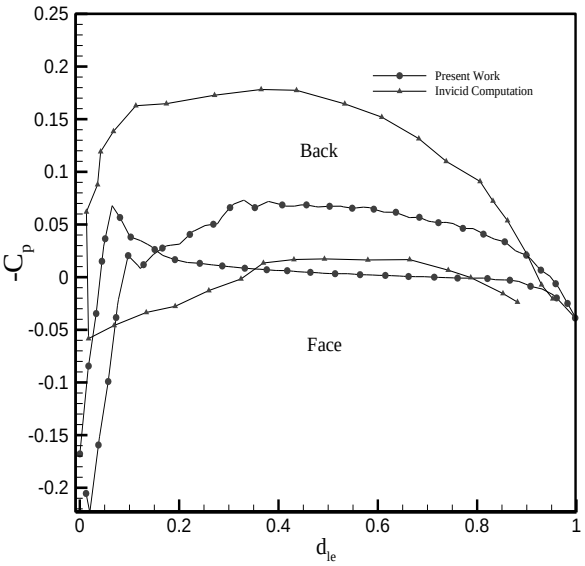

Fig. 9. The variations of the pressure coefficient in the section of $d_r = 0.5$

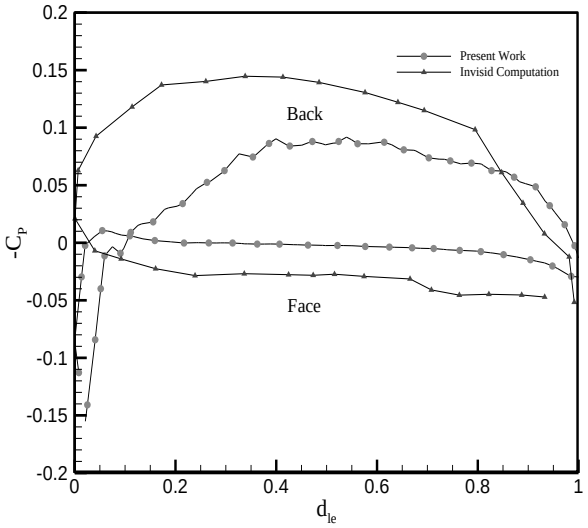

Fig. 10. The variations of the pressure coefficient in the section of $d_r = 0.7$

4.3. Variations of the Pressure Coefficient

Figures 9 and 10 displayed the variations of the pressure coefficient on the sections with d_r of 0.5 and 0.7 on the blades of the propeller ($d_r = \frac{r}{R}$). r was the radial distance from the propeller hub and R was the propeller radius. Furthermore, the horizontal axis of the figures was the d_{le} parameter, which showed the distance from the leading edge at the section of propeller blade. Moreover, it was worth mentioning that the pressure coefficients were calculated based on J = 0.83. The value of the pressure coefficient in these sections was obtained based on the following equation:

$$C_p = \frac{2p - 2p_0}{\rho v_0^2 \left[1 + (\frac{\pi d_r}{J})^2\right]} \quad (14)$$

where p_0 is the reference pressure and v_0 is the forward velocity of the propeller.

In Fig.10, the pressure coefficient at first decreases and then augments, as it moves from the leading edge to trailing edge in the suction surface. Moreover, by increasing the blade radius and its speed, the minimum pressure increased in a way that pressure coefficient reached its minimum value.

The pressure coefficient contours on all the surfaces are shown in Figs. 11 and 12. As can be concluded from these figures, the pressure coefficient increased and the blade radius got augmented as it moves from the leading edge to trailing edge in the pressure surface. Furthermore, the pressure coefficient also increased.

The surfaces with the same velocity and vorticity are shown in Fig. 13. As can be seen in these plots, the propeller was inclined to move toward the axial direction rather than the radial direction.

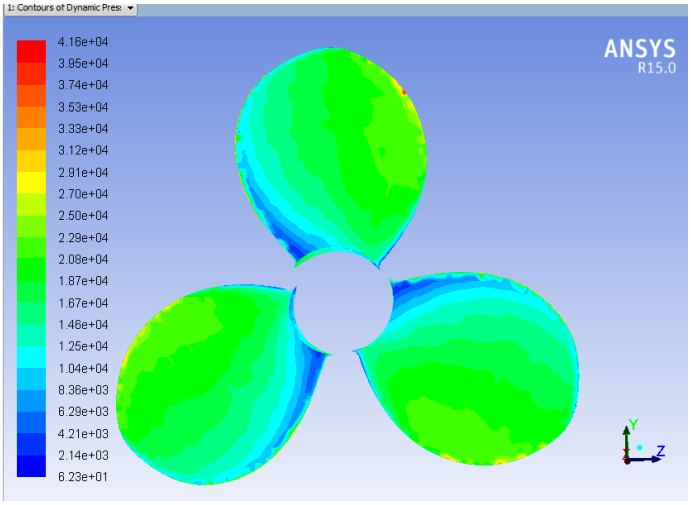

Fig. 11. The pressure coefficient contour on suction surface

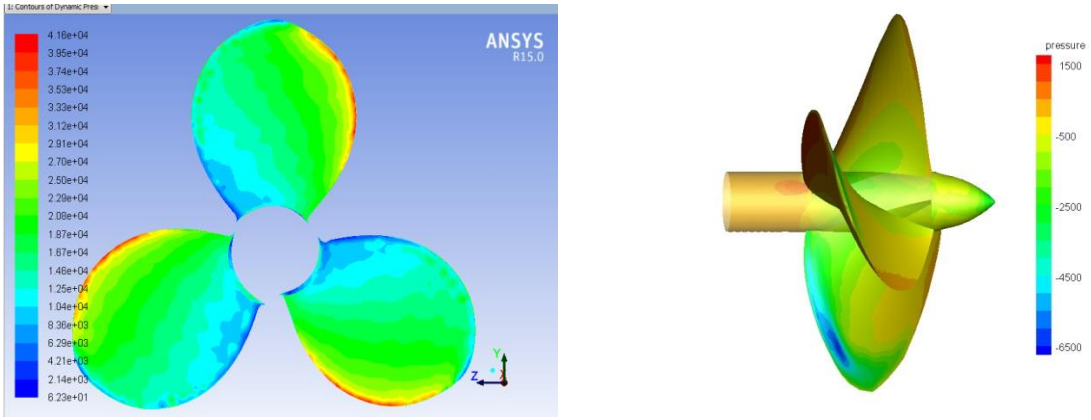

Fig. 12. The pressure coefficient contour on pressure surface

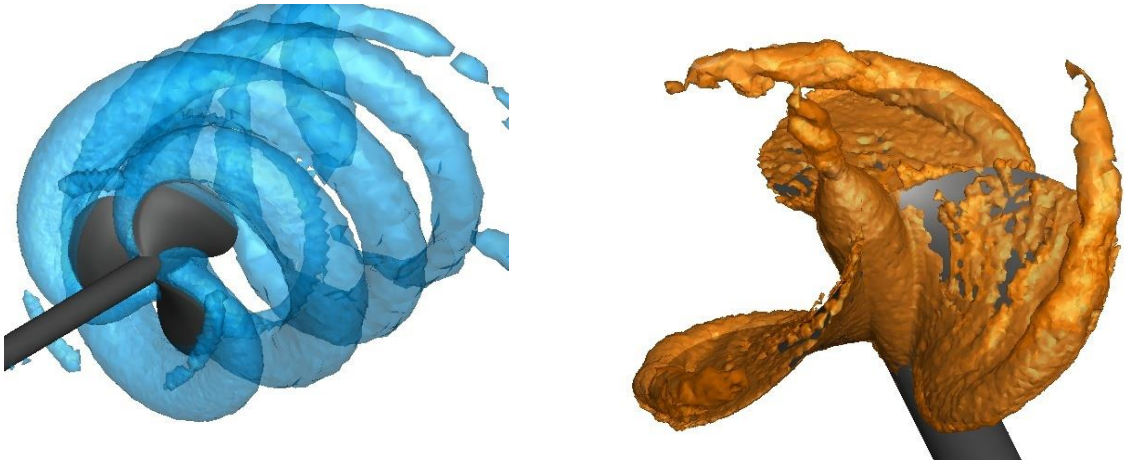

Fig. 13. The surfaces with the same velocity and vorticity for the DTMB4119 propeller

4.4. Cavitation around the Propeller

The volume of the formed vapor in three considered cord radius is shown in Fig.14. As can be seen in this figure, the maximum volume of the vapor was formed in 0.747R. The volume fraction of the vapor over the blades in different advance coefficients was indicated in Figs. 15–17. According to these figures, as the advance coefficient increased, the volume fraction of the vapor over the blades diminished.

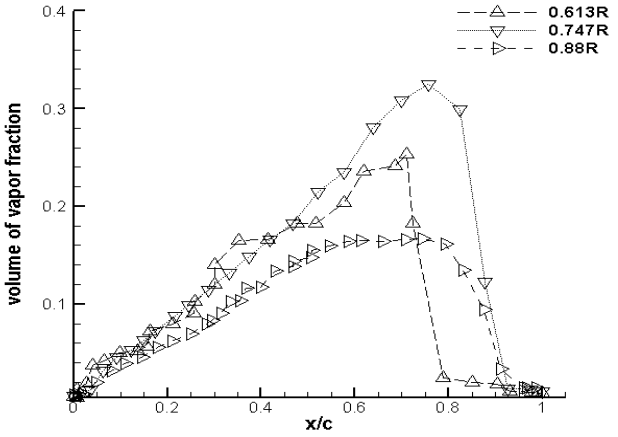

Fig. 14. The volume of the formed vapor in three considered cord radius

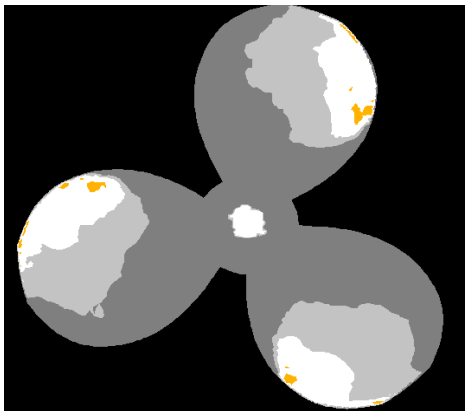

Fig. 15. The volume fraction of the vapor over the blades in j = 0.6

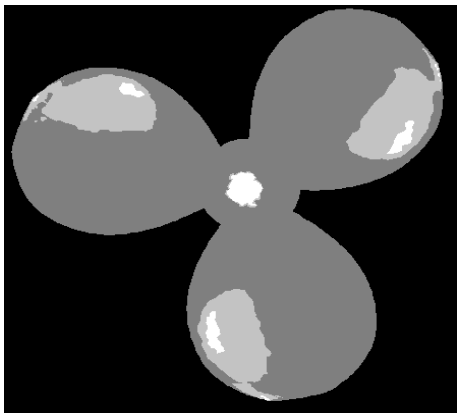

Fig. 16. The volume fraction of the vapor over the blades in j = 0.7

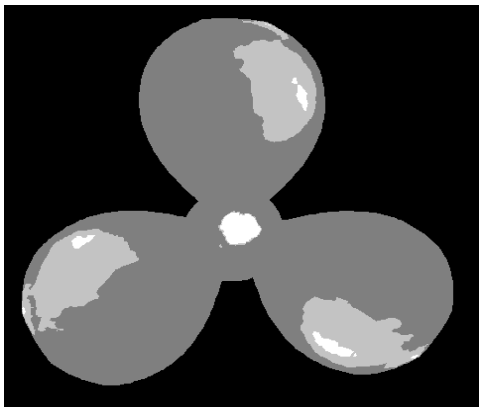

Fig. 17. The volume fraction of the vapor over the blades in j = 0.833

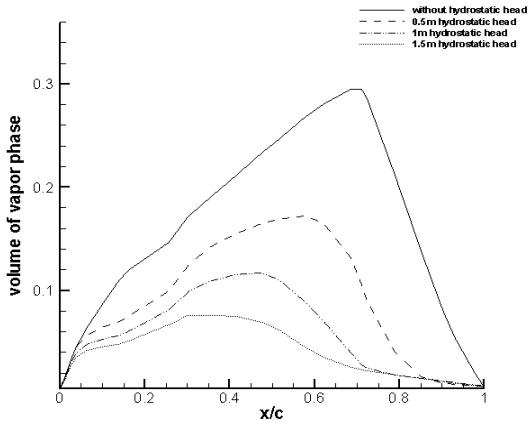

Fig. 18. The volume of vapor phase in terms of variation of hydrostatic head in 0.613 radius

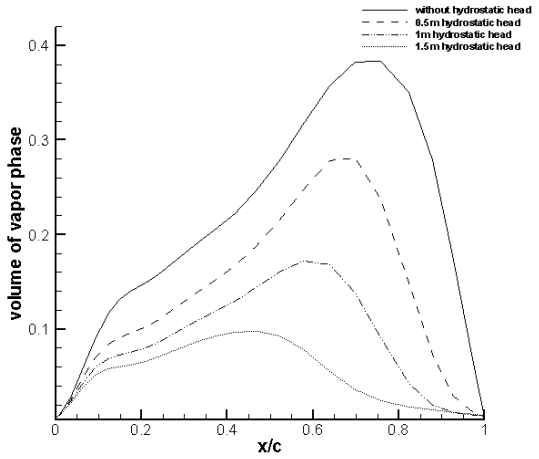

Fig. 19. The volume of vapor phase in terms of variation of hydrostatic head in 0.747 radius

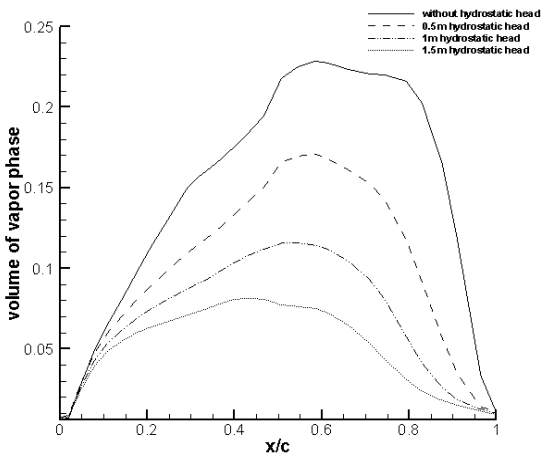

Fig. 20. The volume of vapor phase in terms of variation of hydrostatic head in 0.88 radius

5. Conclusion

In the current study, a numerical simulation was conducted to investigate the behavior of the DTMB4119 propeller in the open water condition. The ANSYS-FLUENT packages were employed to exploit the results. The propeller hydroacoustics was produced by vorticities, in which these vorticities were created by rotating the propeller. The non-cavitation propeller noise came from dipole. In this study, propeller was simulated in cavitation and non-cavitation conditions. As it was seen, in this research, we could simulate the produced vorticities, which were the principle factor in propeller hydroacoustics. Moreover, they were significant factors in designing the propellers. The results showed that by moving from the leading edge to trailing edge in the suction surface, the pressure coefficient at first decreased and then got augmented. Moreover, by increasing the blade radius and its speed, the minimum pressure increased in a way that pressure coefficient reached its minimum value. Furthermore, by moving from the leading edge to trailing edge in the pressure surface, the pressure coefficient increased and the blade radius got augmented, increasing the pressure coefficient. Furthermore, as the advance coefficient increased, the volume fraction of the vapor over the blades decreased. As a result, the possibility of occurring cavitation decreased.

Reference

[1] Kulczyk J., Skraburski Ł., M. Zawislak, Analysis of Screw Propeller 4119 Using the Fluent System, Archives of Civil and Mechanical Engineering (2007) 7: 129-137.

[2] Mirjalili S., Lewis A., Mirjalili S. A. M., Multi-Objective Optimisation of Marine Propellers, Procedia Computer Science (2015) 51: 2247-2256

[3] Krasilnikov V., Sun J., Halse K. H., CFD Investigation in Scale Effect on Propellers with Different Magnitude of Skew in Turbulent Flow, In The First International Symposium on Marine Propulsors, Trondheim (2009) 25-40.

[4] Nakisa M., Abbasi M. J., Amini A. M., Assessment of Marine Propeller Hydrodynamic Performance in Open Water via CFD, in Proceedings of The 7th International Conference on Marine Technology (MARTEC 2010) (2010).

[5] Kerwin J. E., Lee C.-S., Prediction of Steady and Unsteady Marine Propeller Performance by Numerical Lifting-Surface Theory (1978).

[6] Chang B. J., Application of CFD to P4119 Propeller, In 22nd ITTC Propeller RANS/Panel Method Workshop, France (1998).

[7] Funeno I., Analysis of Unsteady Viscous Flows around a Highly Skewed Propeller, Journal of Kansai Society of Naval Architects (2002) 237: 39-45.

[8] Hu X.-f., Huang Z.-y., Hong F.-w., Unsteady Hydrodynamics Forces of Propeller Predicted with Viscous CFD [J], Journal of Hydrodynamics (Ser. A) (2009) 6: 010.

[9] Ekinci S., Celik F., Guner M., A Practical Noise Prediction Method for Cavitating Marine Propellers, Brodogradnja (2010) 61:359-366.

[10] Huang S., Zhu X.-y., Guo C.-y., Chang X., CFD Simulation of Propeller and Rudder Performance when Using Additional Thrust Fins, Journal of Marine Science and Application (2007)6: 27-31.

[11] Da-Qing L., Validation of RANS Predictions of Open Water Performance of a Highly Skewed

Propeller with Experiments, Journal of Hydrodynamics (2006) 18: 520-528.
[12] Atsavapranee P., Miller R., Day C., Klamo J., Fry D., Steady-Turning Experiments and RANS Simulations on a Surface Combatant Hull form (Model#5617), In Proceedings of 28th symposium on naval hydrodynamics, Pasadena, California (2010).
[13] Kulczyk J., Skraburski L., Zawislak M., Analysis of Screw Propeller 4119 Using Fluent System, Archives of Civil and Mechanical Engineering (2007)7(4):139–150.
[14] Shih T.-H., Liou W.W., Shabbir A., Yang Z., Zhu J., A New k- ε Eddy-Viscosity Model for High Reynolds Number Turbulent Flows - Model Development and Validation", Computers Fluids (1995) 24(3): 227–238.
[15] Menter F.R., Review of the SST Turbulence Model Experience from an Industrial Perspective, International Journal of Computational Fluid Dynamics (2009)23(4):305-316.
[16] Mohammadi B., Pironneau O., Analysis of the K-Epsilon Turbulence Model (1993).
[17] Orszag S. A., Yakhot V., Flannery W. S., Boysan F., Choudhury D., Maruzewski J., Renormalization Group Modeling and Turbulence Simulations, Near-Wall Turbulent Flows (1993)1031-1046.
[18] Chima R., A k-Omega Turbulence Model for Quasi- Three- Dimensional Turbomachinery Flows, In 34th Aerospace Sciences Meeting and Exhibit (1995) 248.